Supplementary material for:

Activation of palindromes on a degradable modular grafting probe enables ultrasensitive detection of microRNAs

Jianguo Xu[1*], Zhi Li[3], Yumei Li[3], Yusheng Lu[3], and Jie Wang[2, 3*]

[1]School of Food Science and Biological Engineering, Hefei University of Technology, Hefei 230009, China

[2]School of Pharmacy, Anhui Medical University, Hefei 230031, China

[3]College of Chemistry, Fuzhou University, Fuzhou 350002, China.

*Correspondence should be addressed to E–mail:

jgxu0816@163.com (J. G. Xu)&wangjienar@163.com (J. Wang)

ORCID: 0000-0002-0187-2623(J. G. Xu)

Experimental section

Reagents

All oligonucleotides were synthesized and purified by Sunya Biotechnology Co., Ltd. (Fuzhou, China). Their sequences are summarized in **Table S1**. Prior to use, they were dissolved in 1×TE (10 mM Tris-HCl, 1 mM EDTA, pH=7.4) with a storing concentration of 10 μM. Enzymes of phi29-poly, klenow fragment (3'-5'exo$^-$) polymerase, and Nt.BbvCI-nick were ordered from New England Biolabs (Beijing, China). T4 DNA polymerase was from Shanghai Sangon Biological Engineering Technology and Services Co., Ltd. (Shanghai, China). All reagents were of analytical grade and used without further purification. Ultrapure water (Resistance= 18 MΩ/cm) was obtained by a Kerton lab MINI water purification system (UK).

Instrument

Fluorescent measurements were done by a fluorescence spectrophotometer (FL-7000, Shimadzu, Japan) with an excitation wavelength at 492 nm (slit= 5 nm), the slit for emission is 5 nm, a scanning speed of 600 nm/min, and a PMT detector voltage of 500V. Emission spectra were recorded from 500-600 nm and the peak fluorescence intensity at 520 nm was employed to evaluate the assay performance. Controlling of reaction temperature was conducted on a TU-200 Block Heater (Yiheng Co. Ltd., Shanghai, China). To characterize the amplification mechanism, prepared DNA samples were run on a 12% PAGE gel with 0.5× TBE buffer (44.5 mM Tris-H_3BO_3, 1 mM EDTA, pH=8.3) and stained with SGI. Imaging of bands was on a Bio-rad ChemDoc XRS with Image Lab software (Bio-Rad, USA).

Ultrasensitive analysis of miRNAs by MGP^{21} induced amplification

To carry out the miRNA-21 determination, a total volume of 50 μL reaction mixture containing 2.5 μL of 2 μM MGP^{21}, 2.5 μL of miRNA-21 at a certain concentration, 5 μL of 10 μM 10×phi29-poly buffer, 1 μL of 10 mM dNTPs, 0.5 μL of 10 U/μL phi29-polymerase, 0.5 μL of 10 U/μL Nt. BbvCI-nick, and 38 μL of ultrapure water were incubated at 37 ℃ via a metal bath for 2 h. Thereafter, 149 μL of ultrapure water and 1 μL of SGI (10×) were added to the reaction system. Followed by a thorough mixing,

the obtained mixture was directly used for fluorescence recording.

Cell culture, total RNA extraction, and RT-qPCR amplification

Hela (Human cervical cancer cell line) and MCF-7 cells (human breast adenocarcinoma cell line) were supplied from Chinese Academy of Sciences (Shanghai). They were cultured in Dulbecco's modified Eagle's culturing medium containing 10% fetal bovine serum, 100 U/mL penicillin, and 100 mg/mL streptomycin. At the exponential growth phase, the cells were harvested and treated with the Trizol reagent (Invitrogen) to extract total RNAs according to the manufacture's instruction.

Prior to conduct the RT-qPCR amplification for miRNA-21 detection, a specifically designed stem-loop reverse transcription primer was prepared with referenced sequence as follows: "5'-GTCGTATCCAGTGCAGGGTCCGAGGTATTCGCACTGGATACGACTCAACA TCAGTCTGATAAGCTA-3"[1]. Thereafter, a two-step (reverse transcription and amplification) qRT-PCR was performed using the PrimeScriptTM RT reagent Kit (Takara, China). U6 RNA with reverse transcription primer of 5'-AACGCTTCACGAATTTGCGT-3' served as the internal reference. In brief, the reverse transcription was implemented at 42℃ for 15 min. The subsequent amplification began with an initial denaturation at 95 °C for 30 s and then set with a thermal process consisted of 40 cycles (95 °C for 30 s, and 60 °C for 30 s), and a final extension at 72 °C for 7 min. The amplification primers for miRNA-21 are 5'-GCCGCTAGCTTATCAGACTGATGT-3' (forward primer) and 5'-GTGCAGGGTCCGAGGT-3' (reverse primer), while the amplification primers for U6 RNA are 5'-CTCGCTTCGGCAGCACA-3' (forward primer) and 5'-AACGCTTCACGAATTTGCGT-3' (reverse primer).

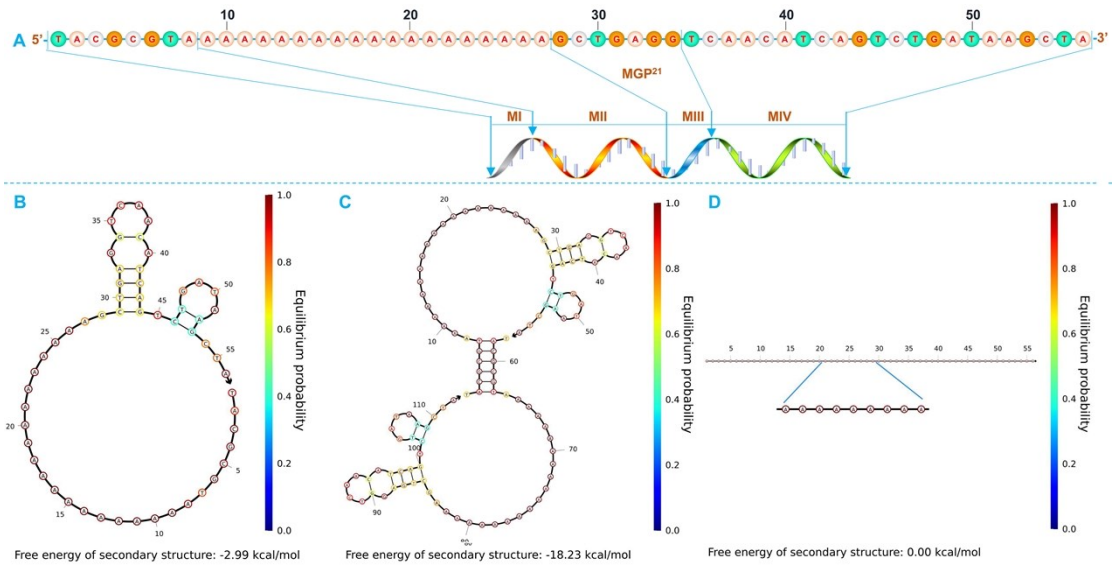

Figure S1. Modular analysis of MGP^{21} (A). Predicted secondary structure of MGP^{21} (B), MGP^{21}/MGP^{21} (C), and ARP (D) by a "NUPACK" software. The free energy of MGP^{21} (-2.99 kcal/mol) indicates it's almost single-stranded. The free energy of MGP^{21}/MGP^{21} (-18.23 kcal/mol) indicates the possibility of intermolecular palindrome pairing. The free energy of ARP (0.00 kcal/mol) indicates it's absolutely single-stranded.

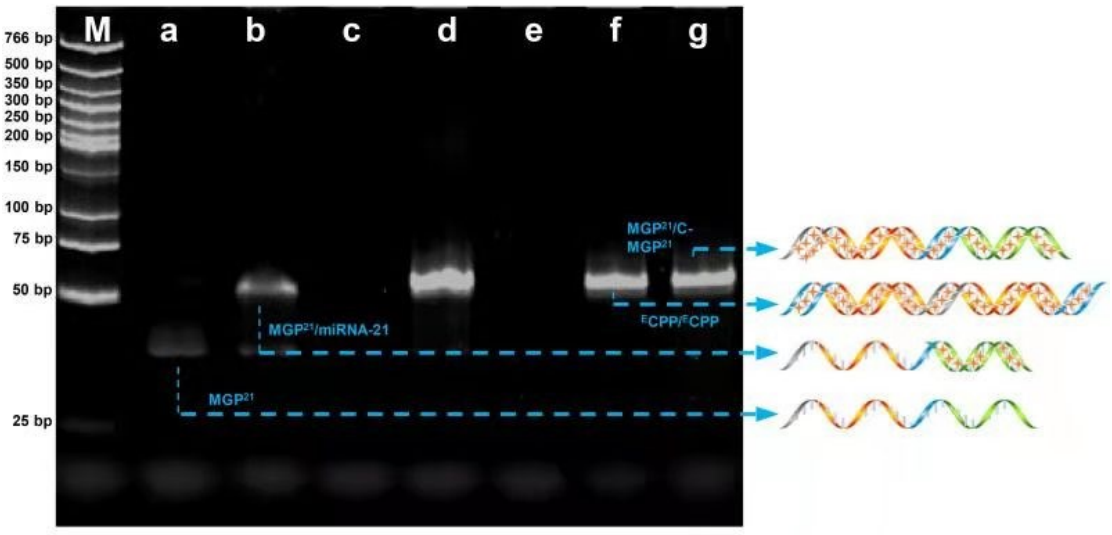

Figure S2. Gel electrophoresis characterization of (a) MGP^{21}, (b) MGP^{21} and miRNA-21, (c) MGP^{21}, phi29-poly, and Nt.BbvCI-nick, (d) MGP^{21}, miRNA-21, phi29-poly, and Nt.BbvCI-nick, (e) CPP, (f) ^{E}CPP/^{E}CPP, (g) MGP^{21}/C-MGP^{21}. The band of MGP^{21} is very weak in lane a. Hybridization of miRNA-21 with MGP^{21} appears a new retarded band in lane b. Incubation of phi29-poly and Nt.BbvCI-nick with MGP^{21} digest the MGP^{21} band in lane c. In contrast, introduction of miRNA-21 to hybridize MGP^{21} and react with phi29-poly and Nt.BbvCI-nick appears a wide and bright band in lane d, which shows a same position as that of ^{E}CPP/^{E}CPP (56 bp) in lane f and MGP^{21}/C-MGP^{21} (56 bp) in lane g. The CPP band in lane e cannot be visualized due to its very weak secondary structure. These results are strong evidence to validate the amplification mechanism.

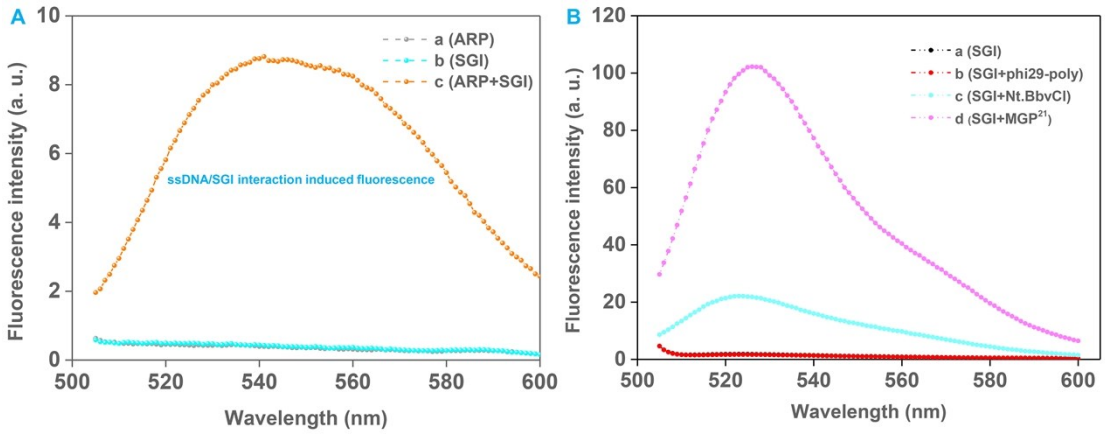

Figure S3. **(A)** Fluorescence responses recorded from ARP (a) and SGI (b) and their mixture (c). [ARP]=100 nM. (B) Fluorescence responses recorded from form (a) SGI, (b) SGI and phi29-poly, (c) SGI and Nt.BbvCl, and (d) SGI and MGP^{21}. [MGP^{21}]=100 nM.

Investigation of the fluorescence background source

To investigate the background source of fluorescence, we prepared the samples of ARP and SGI in Figure S3A. The ARP was absolutely single-stranded. The data verified that although single ARP (curve a) and SGI (curve b) are non-fluorescent, their mixture (curve c) still exhibited a non-negligible fluorescence. Besides, we prepared the samples of SGI before and after added with phi29-poly, Nt.BbvCI, and MGP^{21}, respectively. As shown in **Figure S3B**, incubation of SGI with phi29-poly showed no background signal in curve b, while the incubation of SGI with Nt.BbvCl induced a weak background in curve c. This result indicates using SGI as reporter in some sensing systems, the background source of fluorescence would also be presumably caused by the insertion of SGI into some enzyme structures. It is also worthy to be solved. However, the comparison of the curve d and curve c showed the major background was still derived from the SGI/MGP^{21} incubation, which is worthy to be solved at the first place.

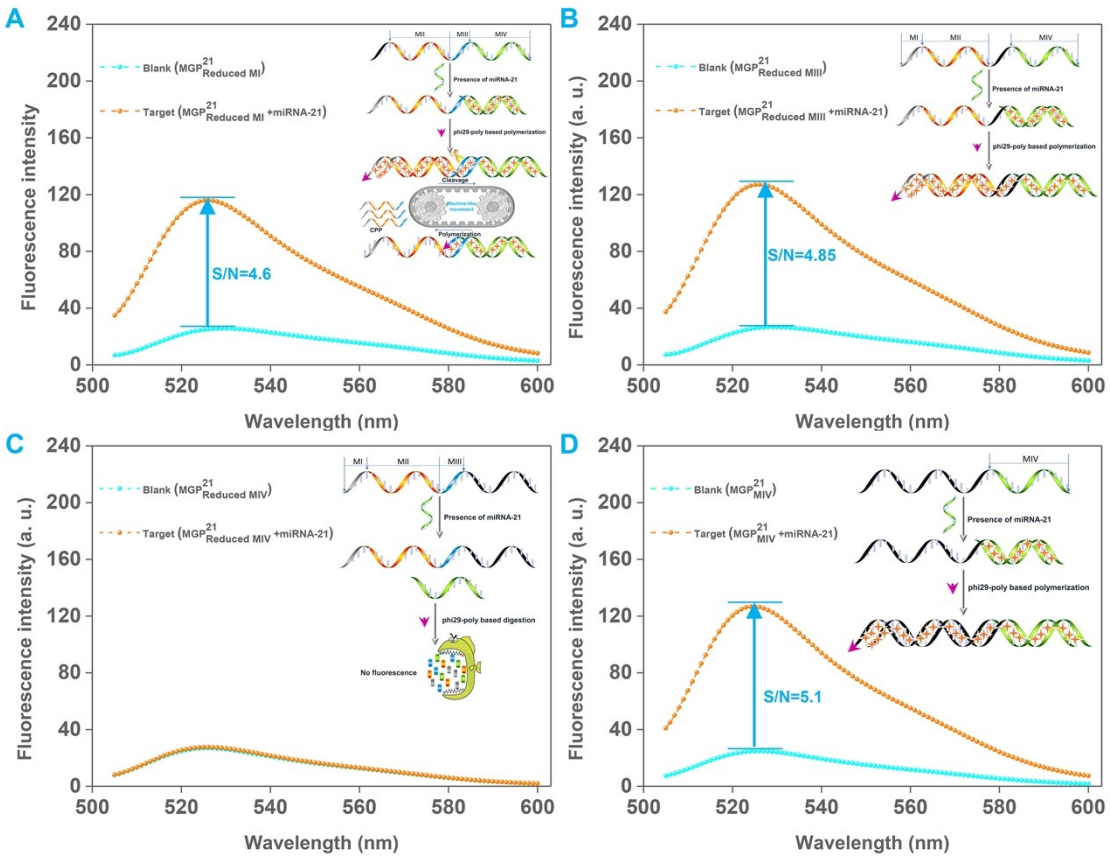

Figure S4. Fluorescent responses of MGP21 Reduced MI (A), MGP21 Reduced MIII (B), MGP21 Reduced MIV (C), and MGP21 MIV (D) based amplification strategies in the absence and presence of target miRNA-21, respectively. Insets are their sensing principles for miRNA-21 analysis. [MGP21 Reduced MI]= [MGP21 Reduced MIII]= [MGP21 Reduced MIV]= [MGP21 MIV]=100 nM, [miRNA-21]=50 nM.

Comparative study between MGP^{21} and its module-reduced probes

Compared with MGP^{21}, MGP21 Reduced MI has no palindromic sequence, MGP21 Reduced MIII is the cleavage site removed counterpart, MGP21 Reduced MIV is designed without the miRNA recognition region, and MGP21 MIV only contains the miRNA recognition module. Their applications for miRNA-21 detection are briefly presented in insert of **Figure S4**. Comparative data in **Figure S4A** revealed that with no palindrome (MI) to produce activated palindromic primers, no ^{E}CPP/^{E}CPP duplexes in the MGP21 Reduced MI based amplification can be collected to bind with SGI, resulting in a compromised S/N ratio of 4.6 lower than that of MGP^{21} in **Figure 1**. Similarly, due to the lack of cleavage site (MIII) in **Figure S4B**, the Nt.BbvCI-nick

cannot work anymore and in turn deteriorate the machine-like amplification to produce CPPs. As a result, the MGP21 Reduced MIII based amplification only achieved a low S/N ratio of 4.85. For MGP21 Reduced MIV based system, the missing of the prerequisite of target hybridization (MIV) led to that no matter the target miRNA was presented or not, the MGP21 Reduced MIV will be completely degraded so that it was unable to amplified sensing miRNA-21. The almost overlapping of the blank and target spectra in **Figure S4C** confirms this expectation. In addition, the simple retaining of the miRNA recognition region made the MGP21 MIV based amplification in **Figure S4D** was very similar to that of MGP21 Reduced MIII based amplification. The MII is not explored since it is not specially functionalized. The results shows each module is an indispensable element and should be strictly obeyed.

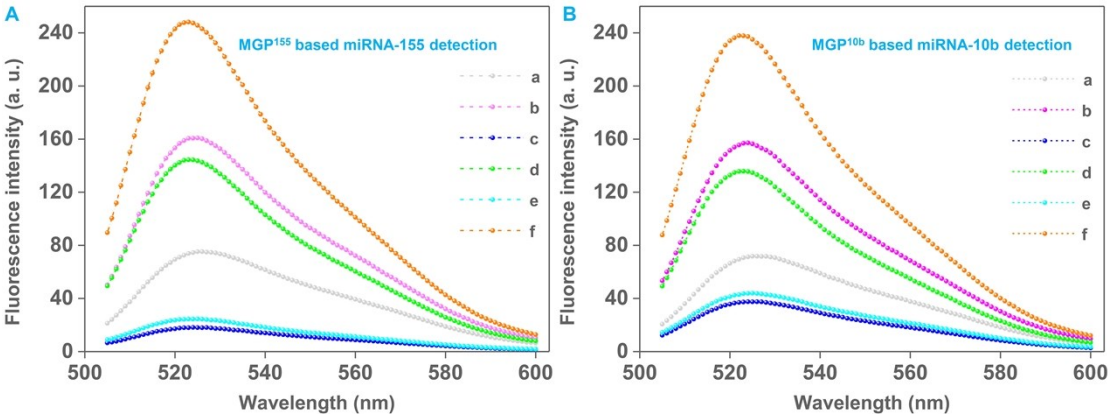

Figure S5. (A) Fluorescent measurements of MGP^{155} (a); MGP^{155} and miRNA-155 (b); MGP^{155} and phi29-poly (c); MGP^{155}, phi29-poly, and miRNA-155 (d); MGP^{155}, phi29-poly, and Nt.BbvCI-nick (e); and MGP^{155}, phi29-poly, Nt.BbvCI-nick, and miRNA-155 (f). [MGP^{155}]=100 nM, [miRNA-155]=50 nM. (B) Fluorescent measurements of MGP^{10b} (a); MGP^{10b} and miRNA-10b (b); MGP^{10b} and phi29-poly (c); MGP^{10b}, phi29-poly, and miRNA-10b (d); MGP^{10b}, phi29-poly, and Nt.BbvCI-nick (e); and MGP^{10b}, phi29-poly, Nt.BbvCI-nick, and miRNA-10b (f). [MGP^{155}]=100 nM, [miRNA-10b]=50 nM.

Universality demonstration

To demonstrate the universality for probing other miRNAs, MGP^{155} and MGP^{10b} are designed according to the design rule of MGP^{21}. It is noticeable that the spectra change trends of the MGP^{155} group and MGP^{10b} group in **Figure S5** are identical to the MGP^{21} group in **Figure 1**, suggesting the target analytes of miRNA-155 (Figure S5A) and miRNA-10b (Figure S5B) can be sensitively probed by MGP155 and MGP10b, respectively.

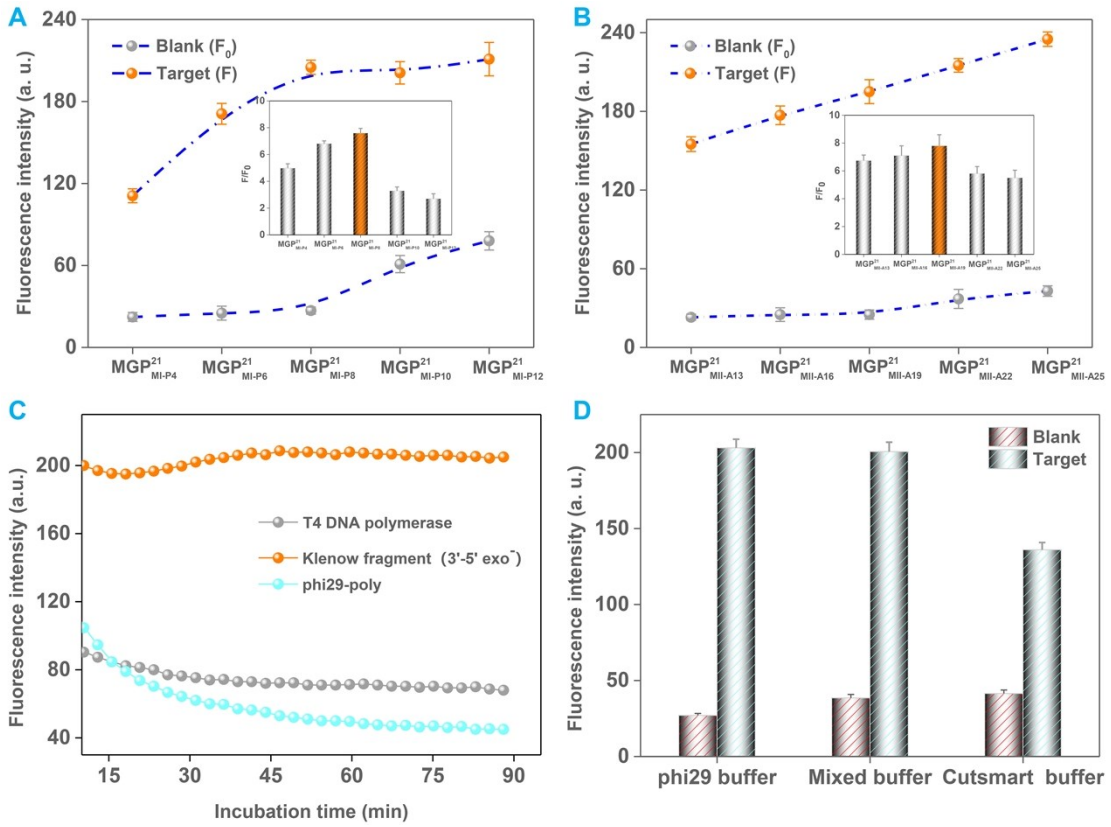

Figure S6. Effects of (A) the base number of MI (palindromic sequence), (B) the base number of MII (A-rich strand), (C) the kind of polymerase, and (D) the kind of reaction buffer on the assay performance. [MGP21 MI-P4]=[MGP21 MI-P6]=[MGP21 MI-P8]=[MGP21 MI-P10]=[MGP21 MI-P12]=[MGP21 MII-A13]=[MGP21 MII-A16]=[MGP21 MII-A19]= [MGP21 MII-A22]=[MGP21 MII-A25]=100 nM. [miRNA-21]=50 nM. [klenow polymerase (3'-5' exo-)]=[phi29-poly]= [T4 DNA polymerase]=0.5 U.

Optimization of experimental conditions

To achieve best assay performance, several parameters including the base number of MI (palindromic sequence), the base number of MII (A-rich strand), the kind of polymerase, and the kind of reaction buffer are optimized in **Figure S6**. In **Figure S6A**, five different MGPs with palindromic base number of 4 (MGP21 MI-P4), 6 (MGP21 MI-P6), 8 (MGP21 MI-P8), 10 (MGP21 MI-P10), and 12 (MGP21 MI-P12) were designed to test the effect of palindromic sequence on the output signal. One can find that the increase of the palindromic base number induced both the increase of blank signal and target signal. The optimal one is MGP21 MI-P8 since it can get maximum

S/N ratio (seen in inset). Likewise, the optimization of MII showed that the MGP21 MII-A19 performed a better sensing capacity than MGP21 MII-A13, MGP21 MII-A16, MGP21 MII-A19, MGP21 MII-A22, and MGP21 MII-A25 in **Figure S6B**. Accordingly, MGP21 MII-A19 is adopted as the optimal probe. Of note, the sequences of MIII and MIV are not optimized since they have fixed bases. On the basis of **Figure S6A** and **S6B**, the detail sequence of MGP^{21} ("TACGCGTAAAAAAAAAAAAAAAAAAAAGCTGAGGTCAACATCAGTCTG ATAAGCTA") is thus presented for us. **Figure S6C** and **S6D** then investigated the polymerase and reaction buffer, respectively. As shown in **Figure S6C**, with the increasing of incubation time, the klenow polymerase (3'-5' exo-) cannot decrease the background signal of SGI/MGP^{21} because of the lack of the 3'-5' proofreading ability of klenow polymerase (3'-5' exo-). The phi29-poly showed a strong degradation ability than T4 DNA polymerase to degrade MGP^{21}. In fact, the gradual decreased signal is a reflect of the digestion of MGP^{21}. Accordingly, the phi29-poly was used in this work. **Figure S6D** recorded the difference using different buffers to carry out the determination of same concentration miRNA-21. The lowest background and highest target response were obtained in the 10×phi29 buffer (500 mM Tris-HCl, 100 mM $MgCl_2$, 100 mM $(NH_4)_2S0_4$, 40 mM DTT, pH7.5), which is provided with the phi29-poly. The 10×CutSmart buffer (500 mM Potassium Acetate, 200 mM Tris-acetate, 100 mM Magnesium Acetate, 1000 μg/ml BSA, pH 7.9) provided with the Nt.BbvCI-nick or the coupling use of phi 29 buffer and CutSmart buffer (1:1, v/v) affected the S/N value.

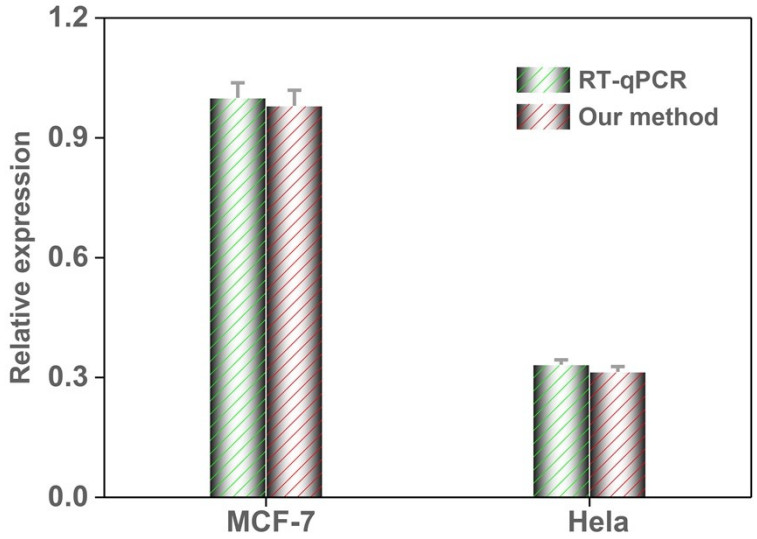

Figure S7. Real samples analysis. MiRNA-21 levels determined using our proposed method in MCF-7 cell and Hela cells compared with the RT-qPCR. Error bars are from three independent experiments.

Real sample analysis

We finally applied the method to detect the relative expression level of miRNA-21 in MCF-7 and Hela cells. The standard method of RT-qPCR severs as the control. As displayed in **Figure S7**, our method showed the expression level of miRNA-21 in MCF-7 (6.87 pM) is much higher than Hela (2.07 pM), which matches very well with the RT-qPCR data and also is consistent with previous reports[2, 3]. As a result, this comparison convinces the practicability of the MGP21 based detection method for analysis of real samples.

Table S1. Oligonucleotides used in the current study.

Note	Sequence (5'-3')
MGP^{21}	TACGCGTAAAAAAAAAAAAAAAAAAAAGCTGAGGTCAACATCAGTCTGATAAGCTA
miRNA-21	UAGCUUAUCAGACUGAUGUUGA
$MGP^{21}_{Reduced\ MI}$	AAAAAAAAAAAAAAAAAAAAAAAAAAAAGCTGAGGTCAACATCAGTCTGATAAGCTA
$MGP^{21}_{Reduced\ MIII}$	TACGCGTAAAAAAAAAAAAAAAAAAAAAAAAAAAATCAACATCAGTCTGATAAGCTA
$MGP^{21}_{Reduced\ MIV}$	TACGCGTAAAAAAAAAAAAAAAAAAAAGCTGAGGAAAAAAAAAAAAAAAAAAAA
MGP^{21}_{MIV}	AAAAAAAAAAAAAAAAAAAAAAAAAAAAAAAAAAAATCAACATCAGTCTGATAAGCTA
MGP^{21}_{MI-P4}	CGCGAAAAAAAAAAAAAAAAAAGCTGAGGTCAACATCAGTCTGATAAGCTA
MGP^{21}_{MI-P6}	ACGCGTAAAAAAAAAAAAAAAAAAAAGCTGAGGTCAACATCAGTCTGATAAGCTA
MGP^{21}_{MI-P8}	TACGCGTAAAAAAAAAAAAAAAAAAAAGCTGAGGTCAACATCAGTCTGATAAGCTA
MGP^{21}_{MI-P10}	CTACGCGTAGAAAAAAAAAAAAAAAAAAGCTGAGGTCAACATCAGTCTGATAAGCTA
MGP^{21}_{MI-P12}	GCTACGCGTAGCAAAAAAAAAAAAAAAAAAGCTGAGGTCAACATCAGTCTGATAAGCTA
$MGP^{21}_{MII-A13}$	TACGCGTAAAAAAAAAAAAAGCTGAGGTCAACATCAGTCTGATAAGCTA
$MGP^{21}_{MII-A16}$	TACGCGTAAAAAAAAAAAAAAAAGCTGAGGTCAACATCAGTCTGATAAGCTA
$MGP^{21}_{MII-A19}$	TACGCGTAAAAAAAAAAAAAAAAAAAGCTGAGGTCAACATCAGTCTGATAAGCTA
$MGP^{21}_{MII-A22}$	TACGCGTAAAAAAAAAAAAAAAAAAAAAAGCTGAGGTCAACATCAGTCTGATAAGCTA
$MGP^{21}_{MII-A25}$	TACGCGTAAAAAAAAAAAAAAAAAAAAAAAAAGCTGAGGTCAACATCAGTCTGATAAGCTA
ARP	AAAAAAAAAAAAAAAAAAAAAAAAAAAAAAAAAAAAAAAAAAAAAAAAAAAAAAAAAAAA
MGP^{155}	TACGCGTAAAAAAAAAAAAAAAAAAAAAGCTGAGGCCCCATCACGATTAGCATTAA
miRNA-155	UUAAUGCUAAUCGUGAUGGGGG
MGP^{10b}	TACGCGTAAAAAAAAAAAAAAAAAAAAGCTGAGGACAAATTCGGTTCTACAGGGTA
miRNA-10b	UACCCUGUAGAACCGAAUUUGU
C-MGP^{21}	TAGCTTATCAGACTGATGTTGACCTCAGCTTTTTTTTTTTTTTTTTTTTTACGCGTA
CPP	TCAGCTTTTTTTTTTTTTTTTTTTTTACGCGTA
^{E}CPP	TCAGCTTTTTTTTTTTTTTTTTTTTTACGCGTAAAAAAAAAAAAAAAAAAAAGCTGA

For MGP^{21}, the grey, red, sky-blue, and green-colored bases indicate the MI, MII, MIII, and MIV, respectively. The MGP^{21} can hybridize with miRNA-21 with its green-colored MIII. MGP21 Reduced MI, MGP21 Reduced MIII, MGP21 Reduced MIV, and MGP21 MIV are the module-reduced counterparts of MGP^{21}. MGP21 MI-P4, MGP21 MI-P6, MGP21 MI-P8, MGP21 MI-P10, and MGP21 MI-P12 are designed with different palindromic base number. MGP21 MII-A13, MGP21 MII-A16, MGP21 MII-A19, MGP21 MII-A22, and MGP21 MII-A25 are designed with different "A" number. The ARP is totally composed of "A" base and has a same base number as MGP^{21}. MGP^{155} and MGP^{10b} are similar designed as MGP^{21}. They can recognize miRNA-155 and miRNA-10b via the blue-colord and purple-colored bases, respectively. C-MGP^{21} is the complementary counterpart of MGP^{21}. CPP is the cleaved product. ^{E}CPP is the extended strand of CPP. During the amplification, the MGP^{21}/C-

MGP[21], CPP, and [E]CPP/[E]CPP are formed.

Table S2. Comparison of different methods for amplified detection of miRNAs.

Methods	Analytes	Linear range	LOD	Orders of amplitude	Ref.
Fluorescent assay	miRNA-155	100 fM-1.0 nM	33.4 fM	5	[4]
Fluorescent assay	miRNA-21	0.05 nM-1 nM	0.01 nM	2	[5]
Fluorescent assay	let-7a	0.05 pM-1 pM	5 fM	2	[6]
Colorimetric assay	miRNA-21	5 fM- 50 pM	5 fM	5	[7]
Electrochemical assay	miRNA-21	10 fM-5 pM	3 fM	3	[8]
Fluorescent assay	let-7a	100 fM-1 nM	21.9 pM	4	[9]
Fluorescent assay	let-7a	100 fM-50 pM	67.3 pM	3	[10]
Electrochemiluminescence assay	miRNA-182	0.1 pM-100 pM	33 fM	3	[11]
Electrochemiluminescence assay	miRNA-21	1 fM-100 pM	0.28 fM	5	[12]
Electrochemiluminescence assay	miRNA-21	1 fM-100 pM	0.65 fM	5	[13]
Fluorescent assay	miRNA-21	1 fM-1 nM	0.26 fM	6	Current study

References

1. C. Chen, D. A. Ridzon, A. J. Broomer, Z. Zhou, D. H. Lee, J. T. Nguyen, M. Barbisin, N. L. Xu, V. R. Mahuvakar, M. R. Andersen, K. Q. Lao, K. J. Livak and K. J. Guegler, *Nucleic Acids Res*, 2005, **33**, e179.
2. J. Xu, C. Yan, X. Wang, B. Yao, J. Lu, G. Liu and W. Chen, *Anal Chem*, 2019, **91**, 9747-9753.
3. X. Chen, K. Xu, J. Li, M. Yang, X. Li, Q. Chen, C. Lu and H. Yang, *Biosens Bioelectron*, 2020, **155**, 112104.
4. X. Miao, Z. Cheng, H. Ma, Z. Li, N. Xue and P. Wang, *Anal Chem*, 2018, **90**, 1098-1103.
5. Y. Zhu, D. Qiu, G. Yang, M. Wang, Q. Zhang, P. Wang, H. Ming, D. Zhang, Y. Yu, G. Zou, R. Badugu and J. R. Lakowicz, *Biosens Bioelectron*, 2016, **85**, 198-204.
6. W. Li, W. Jiang, Y. Ding and L. Wang, *Biosens Bioelectron*, 2015, **71**, 401-406.
7. J. Dong, G. Chen, W. Wang, X. Huang, H. Peng, Q. Pu, F. Du, X. Cui, Y. Deng and Z. Tang, *Anal Chem*, 2018, **90**, 7107-7111.
8. L. Liu, N. Xia, H. Liu, X. Kang, X. Liu, C. Xue and X. He, *Biosens Bioelectron*, 2014, **53**, 399-405.
9. H. H. Sun, F. He, T. Wang, B. C. Yin and B. C. Ye, *Analyst*, 2020, **145**, 5547-5552.
10. X. Tang, R. Deng, Y. Sun, X. Ren, M. Zhou and J. Li, *Anal Chem*, 2018, **90**, 10001-10008.
11. H. Y. Zhu and S. N. Ding, *Biosens Bioelectron*, 2019, **134**, 109-116.
12. Z. Xu, Y. Chang, Y. Chai, H. Wang and R. Yuan, *Anal Chem*, 2019, **91**, 4883-4888.
13. Y. Zhang, G. Xu, G. Lian, F. Luo, Q. Xie, Z. Lin and G. Chen, *Biosens Bioelectron*, 2020, **147**, 111789.